RSC Advances

This is an *Accepted Manuscript*, which has been through the Royal Society of Chemistry peer review process and has been accepted for publication.

Accepted Manuscripts are published online shortly after acceptance, before technical editing, formatting and proof reading. Using this free service, authors can make their results available to the community, in citable form, before we publish the edited article. This *Accepted Manuscript* will be replaced by the edited, formatted and paginated article as soon as this is available.

You can find more information about *Accepted Manuscripts* in the **Information for Authors**.

ROYAL SOCIETY OF CHEMISTRY

www.rsc.org/advances

Synthesis and characterisation of MOF/ionic liquid/chitosan mixed matrix

membranes for CO_2/N_2 separation

Clara Casado-Coterillo[1,*], Ana Fernández-Barquín[1], Beatriz Zornoza[2], Carlos - Téllez[2], Joaquín Coronas[2], Ángel Irabien[1]

[1] *Department of Chemical and Biomolecular Engineering, Universidad de Cantabria,*
Avda. Los Castros s/n, 39005 Santander, Spain

[2] *Department of Chemical and Environmental Engineering and Instituto de Nanociencia*
de Aragón, Universidad de Zaragoza, 50018 Zaragoza, Spain

*Corresponding author: casadoc@unican.es; tel.: +34 942 20 6777.

ABSTRACT

　　　　Mixed matrix membranes (MMMs) have been prepared by combining a small amount of highly absorbing non-toxic ionic liquid, [emim][Ac] (IL) (5 wt.%), a biopolymer from renewable abundant natural resources, chitosan (CS), and nanometre-sized metal-organic framework (MOF) ZIF-8 or HKUST-1 particles to improve the selectivity of the IL-CS hybrid continuous polymer matrix. The TGA revealed that the thermal stability has been enhanced by the influence of both IL and ZIF-8 or HKUST-1 fillers, while keeping a water content of around 20 wt.%, which suggests the potential of such materials for developing high temperature water resistant membranes for CO_2 separation. The CO_2 and N_2 single gas permeation performance was tested at temperatures in the range 25 – 50 ºC, to compare with the previously reported IL-CS

1

hybrid membranes. The best CO_2 permeability and CO_2/N_2 selectivity performance is obtained for 10 wt. % ZIF-8 and 5 wt. % HKUST-1 /IL-CS membranes, as high as 5413 $\pm$ 191 and 11.5, and 4754 $\pm$ 1388 Barrer and 19.3, respectively. This is attributed to a better adhesion and smaller particle size of ZIF-8 than HKUST-1 nanoparticles with respect to the IL-CS continuous matrix, as interpreted by Hansen solubility parameters and Maxwell-based models, modified to account for rigidification, pore blockage and crystallinity of the CS matrix, with very accurate predictions.

Keywords: Mixed matrix membranes; CO_2/N_2 separation, chitosan; ionic liquid; metal organic framework; modelling; Hansen

Introduction

Post-combustion capture to separate CO_2 from flue gas in fossil-fuelled power plants is vital to tackle climate change issues. Although amine absorption is a mature technology widely available at large scale, it presents several drawbacks in post-combustion, regarding steam regeneration, handling of corrosive liquids, amine losses, and the low temperature for efficient separation. Its expensiveness leads to the opportunities for new emerging processes for sustainable CO_2 capture. Membrane separation is a promising alternative to conventional absorption processes because of the simplicity and durability of operation, low footprint and eco-friendliness and potential lower energy cost than amine absorption, all which favour their use at small-scale applications. Although polymeric membranes have been commercialised because of their relatively easy processing at low costs, due to their limited resistance to high

temperature and usual inadequacy to high flow rates or sensitiveness to clogging by dust, there is an absence of economy of scale and low CO_2/N_2 selectivity limitations [1]. Inorganic membranes for CO_2/N_2 separation are inherently microporous based on molecular sieving mechanisms, such as ceramic [2] and zeolite membranes [3]. Permeability and selectivity are the fundamental parameters that characterise the gas separation through membrane materials. There is usually a trade-off between both parameters that was well described by Robeson in his upper bound [4]. At large scale post-combustion capture, however, we have to deal with low CO_2 pressures of 0.15 bar, meaning low driving forces, high permeability becomes crucially important, while high selectivity would avoid pressure ratio dependence of membrane performance [5].

Mixed matrix membranes (MMMs), where the combination of organic and inorganic materials has been proved as a promising way of merging and enhancing the properties of both phases, have been attracting interest in the last decades [6-10]. Recently the MMMs devoted as CO_2 selective have been the object of an extended overview of CO_2 selective membranes [11]. New materials based on renewable resources are most recently sought for to avoid dependency on petroleum-based products. In order to overcome this trade off and obtain membranes with increased permeability and selectivity at the same time, the most important challenge on MMMs is the adhesion or compatibility between the components in order to form a homogeneous film with synergistic properties.

Room temperature ionic liquids (IL) combining good and tuneable solubility properties with negligible vapour pressure and good thermal stability have received much attention as an alternative to the existing CO_2 absorption solvents in membrane contactors. Supported ionic liquid membranes (SILM) were thus proposed to take advantage of high CO_2 absorption of non toxic ILs as a function of the type of anion

was evaluated [12]. The large number of publications dealing with ILs in membranes for CO_2 separation has opened up the field for next generation membranes [8]. In particular, the IL composed of the 1-ethyl-3-methylimidazolium cation and acetate anion, [emim][Ac], is the IL with the highest reported CO_2 solubility even with increased temperature [13], as well as non-reported toxicity [14]. MMMs consisting of polimerizable ionic liquids and free room temperature ILs have been proposed to improve the performance of SAPO-34-based membranes in CO_2/CH_4 separation [15,16], in the light of the outcome of PILs as promising materials for CO_2 capture [17] and polymerized ionic liquids filled with RTILs were also proposed for CO_2/N_2 separation [18], but the selectivity was still low.

Chitosan (CS), poly[β(1→4)-2-amino-2-deoxy- D-glucopyranose], is a linear polysaccharide obtained by deacetylation of chitin, abundant, cheap and acquired from renewable sources, *i.e.* the shell of crustaceans, as well biodegradable, biocompatible, non-toxic and hydrophilic. The high hydrophilicity of CS makes it possible to hydrate and form water-swollen membranes with enhanced CO_2/N_2 permselectivity because of the high CO_2 solubility in water [19]. Swollen CS-based membranes have been studied for CO_2/N_2 separation in facilitated transport, by humidification of the feed gas prior to entering the membrane module [20]. Its mechanical stability has nevertheless been tried to improve by coating on a porous polysulfone support [21], organic chemical crosslinking [22] or physical mixing with zeolite particles [23]. Because of the strong H-bonds forming with OH groups in the polymer chain, ionic liquids are considered as good solvents for polysaccharides [24], and thus a good interaction with ILs was expected. With the aim of increasing mechanical and thermal stability of liquid membranes [25], hybrid solid IL-CS membranes were recently reported by introducing a small amount of [emim][Ac] IL into the CS matrix, leading to a good adhesion with improved flexibility, as well as a

decrease of the influence of temperature on CO_2/N_2 separation [26]. However, the selectivity is still below the Robeson's upper bound [4], by the increased amorphousness imparted by an IL into a semi-crystalline polymer matrix [27]. The incorporation of microporous titanosilicate ETS-10 nanoparticles into CS and IL/CS hybrid matrices was observed to increase tensile strength, and simultaneously and monotonously increased the CO_2/N_2 separation performance by the addition of the same IL and microporous titanosilicate ETS-10 [28] as in other 3-phase MMMs based on PILs, RTILs and molecular sieves [16,17,29].

Metal-organic frameworks (MOFs) have been proposed as promising fillers in MMMs for gas separation because their partly organic nature allows expectation of a higher compatibility with the polymer chains [30]. Adams *et al.* [31] studied a MOF based on copper and terephthalic acid (TPA) that improved the performance of the pure polymer. HKUST-1 or $Cu_3(BTC)_2$ (copper(II)-benzene-1,3,5-tricarboxylate) is a 3D porous metal organic framework (MOF) with high CO_2 sorption ability and thermal stability [32] that was introduced in MMM for gas separation by Car *et al.* [33]. ZIF-8 (Zn(2-methylimidazole)$_2$) belongs to the zeolite imidazole framework subgroup of MOFs with exceptional chemical and thermal stability. ZIF-8 has cavities of 11.6 Å connected through small apertures of 3.4 Å, which makes this material highly studied in hybrid membranes to enhance their molecular sieving ability. Yilmaz and Keskin provided a computational approach that allows developing MOF- and ZIF- based MMMs for CO_2/N_2 separation [34]. ZIF-8 nanoparticles may increase the free volume of low permeability Matrimid polyimide, at the expense of polymer plasticization and loss of selectivity [35]. Both HKUST-1 [36] and ZIF-8 [37] have been used with the aim of improving the plasticization resistance in polyimide membranes for CO_2 separation [29,36,37]. The adsorption capacity of ZIF-8 increases in the presence of water [38]. For CO_2/N_2

separation, there is an urge to match high permeable polymers with intimate mixing fillers that are water and thermally resistant; in this light, ZIF-7 was added to PEBAX and PTMSP permeable polymers to produce a composite membrane with a CO_2 permeability of 145 Barrer and a CO_2/N_2 selectivity of 97 [39]. Recently, as high as 35 % ZIF-8 was loaded into PEBAX forming a dual layer membrane with increased CO_2 permeability and decreased selectivity, but long term stability under humid conditions [40]. The major challenge in MMMs is the adhesion between the phases. Therefore, a ZIF-8 loading of 18.9 wt. % in the ionic polymer p[vbim][NTf$_2$] has been reported to increase the CO_2 permeability of ionic polymer from 101 to 199 Barrer at a constant CO_2/N_2 selectivity of 20, at room temperature [29]. Molecular simulations have been realised using ionic liquids embedded in Cu-BTC to study CO_2/N_2 or CO_2/CH_4 mixtures [41], and the CO_2 adsorption was recently analysed experimentally and validated by molecular simulation [42]. Although small particle size ZIF-8 is better dispersed in the fabrication of MMMs for CO_2/CH_4, still particle modification protocols are needed to increase the selectivity from 19.4 to 28.5 [43].

Therefore, in this work ZIF-8 and HKUST-1 nanoparticles, without the need of particle surface modification, were added at different loadings (5 – 20 wt. %) into the IL-CS hybrid matrix to try to improve the CO_2/N_2 selectivity of the IL-CS hybrid membranes [26]. The 3-phase MMMs were characterised by single gas permeation of CO_2 and N_2 permeabilities as a function of temperature to study the thermal resistance of the membranes. Further characterisation was obtained from TGA, XRD and SEM. The transport properties were fitted to Maxwell-based models as a function of temperature, type of filler and membrane morphology.

Materials and Methods

Materials

Chitosan (CS, coarse ground flakes and powder, Sigma-Aldrich) with a deacetylation degree higher than 75 wt. % and high viscosity in 1 wt. % acetic acid/water was used as purchased. This CS product provides high density of amino groups for CO_2 separation [20].

Zeolite imidazole framework (ZIF-8) nanocrystals were prepared in aqueous solution as reported elsewhere [44,45]. HKUST-1 or $Cu_3(BTC)_2$ powder was also prepared by a procedure described elsewhere [46,47]. The average particle size and morphology observed by SEM are shown in **Figure 1**, giving average values of 0.16 ± 0.02 µm and 0.34 ± 0.20 µm for ZIF-8 and HKUST-1, respectively, from a total measured population of 45 particles.
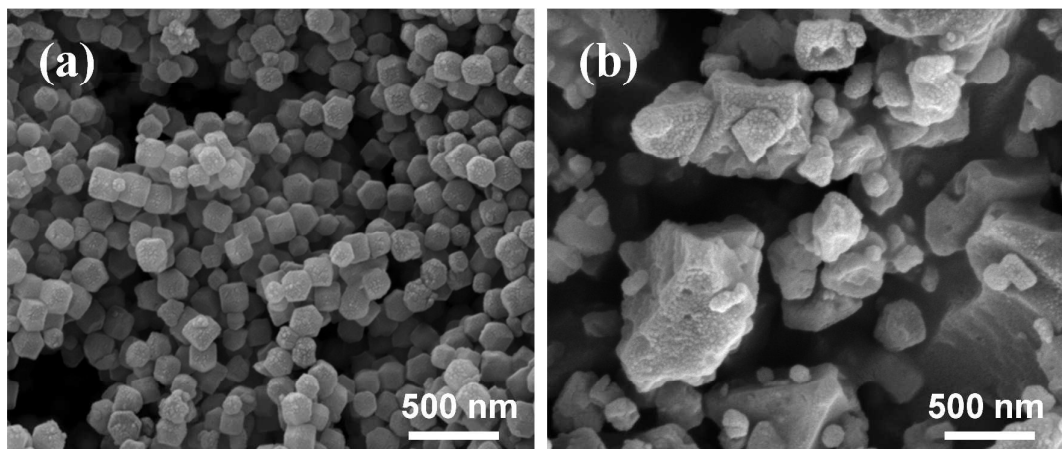
Figure 1. SEM images of the ZIF-8 (a) and HKUST-1 (b) particles used in the 3-phase RTIL-CS MMMs.

Methods

The procedure to prepare the MMM has been reported elsewhere [26,28]. In a typical synthesis, CS 1.5 wt. % was first dissolved in 2 wt. % acetic acid (glacial, Panreac) aqueous solutions under stirring at 80 ºC for 24 h under reflux. The CS solution obtained was filtered to remove insoluble impurities. At this point, the ionic liquid (IL, 97 wt. %, Sigma Aldrich) was added in 5 wt. % proportion with respect to the CS concentration in the solution, which was deemed the most thermally and mechanically stable in a previous work [26]. The mixture was stirred for 2 h. In the case of the MMMs, the HKUST-1 or ZIF-8 nanoparticle filler was first stirred in a 2-3 mL DI water before addition to the IL-CS solution, in $5 - 20$ wt. % content with respect to the total IL-CS organic composition, to study the influence of filler loading on membrane performance. Then, the 10 mL hybrid solution was stirred for 24 h and degassed in an ultrasound bath, then cast on a polystyrene Petri dish and evaporated at room temperature for 2-3 days. The membranes were then removed from the Petri dish. A 14.45 cm^2 membrane was cut from the film for gas permeation and neutralized in 1 M NaOH and rinsed with abundant distilled water. Each membrane was dried at 4 ºC before CO_2 and N_2 permeation experiments to ion exchange the NH_3^+ functional groups of the polymer matrix. Excess of water was carefully removed by blotting with a paper tissue before CO_2 and N_2 permeation tests. Once neutralised with NaOH solutions, there are OH and NH_2 available groups in the chain structure for interaction with CO_2 upon separation performance.

Characterisation

Thicknesses were measured with a IP-65 Digital Micrometer (Mitutoyo Corp. with an accuracy of 0.001 mm). The thicknesses of the membranes were measured in five points over the whole membrane surface before NaOH neutralisation treatment are

collected in **Table 2**, as a function of membrane material composition. The average thickness of all the MMMs prepared in this work range from 90 to 146 μm, although there seems to be a slightly increasing trend with increasing particle loading

The experimental density of the membrane films (ρ_m) was measured gravimetrically from the electronically measured weight of the circular film and the calculated volume of several membranes prepared under the same conditions at room temperature (20 ºC).

Thermogravimetric analyses (TGA) were performed in a DTG 60H Shimadzu instrument in air from 25 – 700 ºC at a heating rate of 10 ºC/min to study the thermal stability of the resulting membranes. The decomposition temperature was calculated as the temperature at which 5 wt. % loss occurs.

The X-ray diffractograms (XRD) of the materials and membranes were collected in the range of 2θ 2.5 – 40º with a step of 0.03º on a D/max 2500 diffractometer (Rigaku, Japan) operating at 40 kV and 80 mA, equipped with rotating Cu anode and a graphite monochromator to select the Cu Kα$_1$ radiation.

The ZIF-8 and HKUST-1 particles and MMMs were characterised by SEM using an Inspect F scanning electron microscope (HITACHI S2300, Japan). In order to observe the cross section of the MMMs, the membranes were fractured by immersion in liquid nitrogen and then 15 nm thick gold sputtered at 10 kV. To evaluate the dispersion of the particles within the membrane matrix, the metal cations were analysed by EDX mapping.

The water uptake of the IL-CS based membranes was measured in membrane pieces of 2 x 2 cm^2, after the neutralisation step in NaOH 1 M and thorough washing in DI water. The membrane pieces were immersed in DI water for 24 h. The wet weight was obtained by quickly blotting the piece of membrane onto a tissue paper to remove

the excess of water. The total water uptake of the membrane material was calculated by the following equation,

$$W_U = 100 \times \left(\frac{w_{wet} - w_{dry}}{w_{dry}} \right) \qquad (1)$$

where w_{dry} is the dry weight of the membrane, which in average was above 0.10 g for accuracy purposes, and w_{wet}, the weight of the swollen membrane (g).

The porosity of the membrane can be calculated from the volume occupied by water and the volume of the membrane, by taking into account the water density at 25 °C (0.997g/cm^3) and the density of the membrane in the dry state [28], which was obtained gravimetrically from the circular membrane used in the permeation experiments. The void fraction, ϕ_v, can thus be calculated as

$$\phi_v = \left(\frac{w_{wet} - w_{dry}}{\rho_{water}} \right) + \frac{w_{dry}}{\rho_{dry}} \qquad (2)$$

where ρ_{dry} is the density of the membrane in the dry state. The water content of the membranes was measured before and after every set of experiments (both gases, temperature range $25 - 50°C$) until constant values, so the gas permeation runs were conducted under constant humid conditions.

Pure N_2 and CO_2 gas permeation was carried out in the home-made constant volume system shown in **Figure 2**, in the temperature interval of $25 - 50$ °C. Membranes were placed in the permeation cell, and tested for N_2 first and then for CO_2. An average of five experimental runs was performed for each membrane composition and only the membranes whose results were reproducible within a 20% error were taken under consideration in this work. In a typical run, both retentate and permeate sides of the membrane module were filled in for a few minutes. Then, all valves were closed and the vent valve was opened to remove the gas in the permeate side and create the driving

force across the membrane. The initial pressure was monitored by a pressure transducer, p_0, and the pressure difference was monitored along the experimental run by differential pressure transducer (Omega, UK), Δp. In total, time an average single membrane spent in the permeation cell along all the experimental runs at least 12h. An average of three single gas permeation experiments for each gas and membrane material were considered to account for reproducibility.
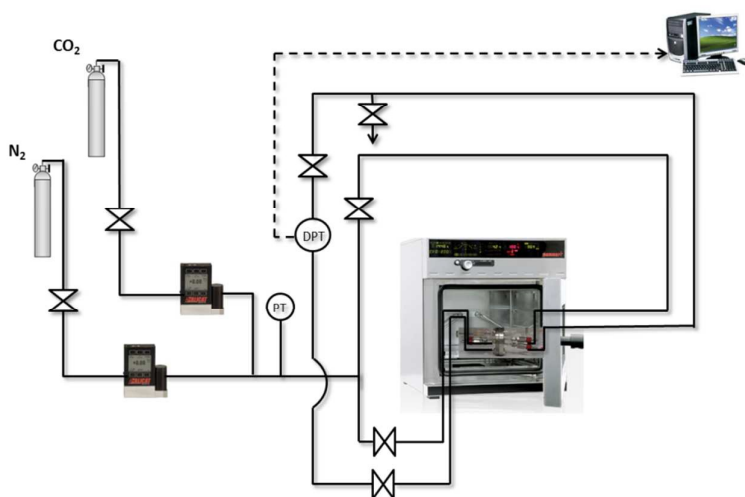
Figure 2. Gas permeation constant volume set up.

The permeability P_i of a pure gas component i through a polymer-based film is defined as follows

$$P_i = \frac{Q_i \cdot l}{A \cdot \Delta p_i} \tag{3}$$

where Q_i is the volumetric gas i (i = CO_2 or N_2, in this work) flowing through the effective membrane area, A, at a Δp_i partial pressure difference, normalized by the membrane thickness, l. P_i is usually given in Barrer (1 Barrer $= 10^{-10}$ cm^3(STP) cm^{-2} s^{-1} cmHg^{-1}), and is a first approximation to the transport properties of a certain membrane material.

11

The transport mechanism across dense polymeric membranes follows the solution-diffusion model,

$$P_i = D_i \times S_i \tag{4}$$

where diffusivity represents the kinetic transport across the membrane, in cm^2/s, and solubility, the thermodynamic affinity of the membrane material for one of the components in the feed mixture, in $cm^3(STP)/cm^3$-cmHg. The diffusivity coefficient is a kinetic term related to the energy necessary for a gas molecule to jump through the polymer matrix and the intrinsic degree of segmental packing. The permeability is calculated at steady state conditions, after the mass balance diffusion using the pressure data in the feed and permeate compartments in the constant volume gas permeation plant drawn in **Figure 2**, leading to eq. (5), according to Cussler [48],

$$ln\left|\frac{\left(p_{i,f}-p_{i,p}\right)_0}{\left(p_{i,f}-p_{i,p}\right)}\right| = ln\left|\frac{\Delta p_0}{\Delta p}\right| = \left(\frac{P_i}{l}\right)\beta_m t \tag{5}$$

where p_f and p_p are the feed and permeate pressure, respectively (Pa), l is the membrane thickness (m), and β_m is a geometric factor (m^{-1}) determined as

$$\beta_m = A_m\left(\frac{1}{V_f} + \frac{1}{V_p}\right) \tag{6}$$

where A_m is the membrane area (m^2), V_p and V_f the permeate and feed compartment volumes (m^3), respectively, with a value of $\beta_m = 110.76$ cm^{-1} in this work.

The solubility S_i correlates with the Hansen solubility parameters (HSP), which are being recently presented as practical tool to predict the material compatibility leading to a good adhesion among the components [49] as well as preferential affinity for CO_2 and N_2 [50]. HSP are based on parameters from the dispersion, polar and hydrogen bonding cohesive energies, respectively, to identify the interaction between the components in a mixture and the gases and the blend, as

12

$$\delta^2 = \left(\frac{E_D}{V}\right)^2 + \left(\frac{E_P}{V}\right)^2 + \left(\frac{E_H}{V}\right)^2 = \delta_D^2 + \delta_P^2 + \delta_H^2 \qquad (7)$$

where δ is the total solubility parameter and V the molar volume, and the parameters are given in $MPa^{1/2}$. This total solubility corresponds to one point in the Hansen space, and the distance between two such points 1 and 2 is given by R_a, as follows,

$$Ra^2 = 4 \cdot \left(\delta_{D1} - \delta_{D2}\right)^2 + \left(\delta_{P1} - \delta_{P2}\right)^2 + \left(\delta_{H1} - \delta_{H2}\right)^2 \qquad (8)$$

The ideal selectivity is the intrinsic parameter describing the ability of a certain membrane material to separate an specific pair of gases and is usually calculated as the ratio of the single gas permeability of the high to low permeating gas, which for the CO_2/N_2 gas pair object of study, is

$$\alpha_{CO_2/N_2} = \frac{P_{CO_2}}{P_{N_2}} \qquad (9)$$

Results and discussion

Figure 3 shows the XRD diffractograms of the materials and membranes studied in this work. The broad peaks around 12 and 20º are attributed to the form I and II of CS pristine polymer, accounting for the semicrystalline nature of CS [28], are discerned in the CS membranes, whereas for the IL-CS membrane these peaks almost disappear. This is attributed to disruption of the semi-crystalline nature upon addition of the IL [51]. The characteristic peaks of ZIF-8 and HKUST-1 are not discerned, not even at the highest loading of 20 wt. %. This can be related to the nanometre size of the filler particles and to the good interaction and mixing at molecular level between the fillers and the CS-based matrix [52]. Hao *et al.* [29] attributed the disappearance of ZIF-8 characteristic peaks

at 7.2 and 10.4º to the destruction of the crystal structure at (001) and (002) by the acid

environment induced by the IL, which in their case was [emim][BF$_4$]. This phenomenon

was probably enhanced by the use of diluted acetic acid solutions employed on the

preparation of the IL-CS-based casting solutions in this work. The ZIF-8 and HKUST-1

loading in the hybrid IL-CS matrix is quite low compared with other MOF MMMs

reported in literature, where only MOF and ZIF loadings of 43 and 60 wt.%,

respectively [53,54], could be observed by XRD therefore the XRD are not conclusive [37].

(a)   **(b)**
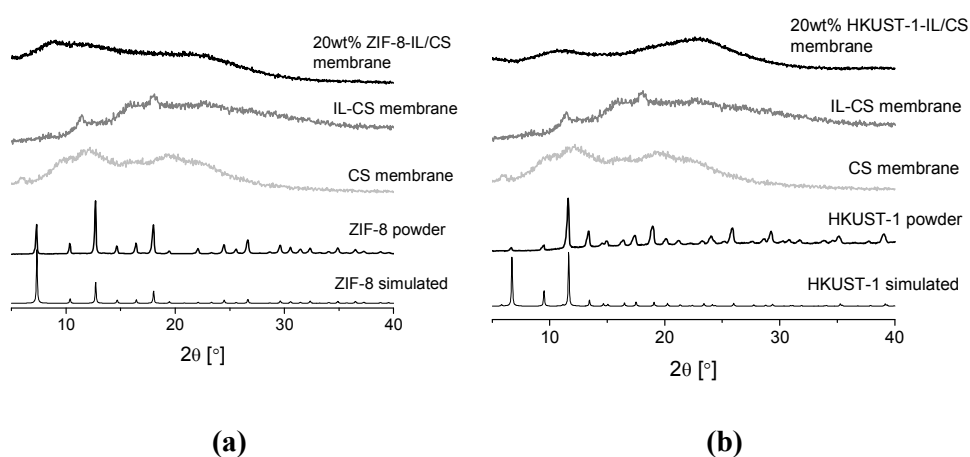
Figure 3. X-ray diffraction patterns of ZIF-8 (a) and HKUST-1 (b) IL-CS based

membranes. ZIF-8 and HKUST-1 powder diffractograms for ZIF-8 and HKUST-1

samples, respectively, are also shown for comparison. Simulated diagrams were

obtained using DIAMOND 3.2k and CIFs 4118891 and 2300380 for ZIF-8 and

HKUST-1, respectively.

The HSP of the materials proposed in this work as components for the hybrid

and MMMs are displayed in **Table 1**. The values of solubility and interaction distance

demonstrate the preferential affinity of the materials for CO_2 vs. N_2, as well as a

relatively good interaction between CS and IL, CS and ZIF-8 and CS and HKUST-1,

even though ZIF-8 is more compatible to CS and IL than HKUST-1. Using the additive

method we can predict the interaction distance of IL-CS-based hybrid membranes, with

CO_2 and N_2 gases in a mixture, as R_a = 20.1 and 30.0 $MPa^{1/2}$, respectively, for IL-CS

membranes. The conclusions of these calculations may be that the CO_2/N_2 separation

performance of IL/CS hybrid membranes could be expected to improve by the addition

of HKUST-1 or ZIF-8 particles, even without additional surface modifiers.

Table 1. Hansen Solubility parameters δ_D, δ_P, δ_H, and δ for pure CS [49], [emim][Ac] IL
[55], HKUST-1 [56], ZIF-8 [57] and the interaction factor R_a with CS and IL (columns A and
B, respectively).

	δ_D (MPa$^{1/2}$)	δ_P (MPa$^{1/2}$)	δ_H (MPa$^{1/2}$)	R_a (-CS) A	R_a (-IL) B
CS	17.8	14.2	24.1	0	11.4
IL	14.2	8.8	17.0	11.4	0
HKUST-1	17.9	9.9	10.7	14.1	9.7
ZIF-8 [a]	20.8	8.6	16.4	11.2	11.8
CO_2	15.7	6.3	5.7	20.5	11.9
N_2	11.9	0	0	30.4	19.7

[a] Because of lack of Hansen' solubility parameters available for ZIF-8, we take the

parameters provided for the 2-methylimidazole (2MI) functional group as the one

responsible in ZIF-8 for interactions with the other components [57].

The smaller the solubility distance parameter R_a between two components, the

better the compatibility. Therefore, since the R_a interaction distances between IL and

ZIF-8 and HKUST-1 are 13.1 and 9.7 $MPa^{1/2}$, respectively, a better ZIF-8/CS adhesion

can be expected in the 3-component MMM. The thermal stability of IL-CS-based membranes in **Figure 4** correlates with the matrix interaction. According to HSP calculations, ZIF-8 is more compatible with CS and IL than HKUST-1, which agrees with the slightly higher thermal stability observed by TGA (**Figure 4**) of ZIF-8/IL-CS MMM than HKUST-1/IL-CS MMM, and Zhu Ryberg *et al.* observations for CS-based nanocomposites [49].

The thermal degradation of the ZIF-8/IL-CS based membranes was measured by TGA in static air in the range 25 to 700 ºC and represented in **Figure 4**. The TGA curves follows the usual three steps of CS thermal degradation: a first step up to 119 ºC corresponds to the removal of free water and is omitted from **Figure 4** to better observe the thermal changes on the new MMMs, taking into account the high water uptake of the CS-based membranes; a second step up to 427 ºC for the removal of bound water and the start of deacetylation of the CS matrix; and a final decomposition step. The weight loss observed before 119 ºC (not shown), as indicated, is attributed to the evaporation of adsorbed water, which increases from 0.22 wt.% for the IL-CS membrane, in agreement with previous results [26,28], to 13.2, 25.4 and 46.1 wt.% for the IL-CS-based membranes filled by 5, 10 and 20 wt.% ZIF-8, respectively. The thermal decomposition temperature is included in **Table 2.** As the ZIF-8 content increased, the thermal decomposition temperature of the IL-CS-based membranes increased from 168 ± 32 ºC to 186 ± 15 ºC when increasing the ZIF-8 content from 5 to 20 wt. %, probably because of the increasing interaction owed to increasing number of H-bonds and decreasing organic content in the membrane matrix [58]. The thermal decomposition of the HKUST-1/IL-CS MMMs is lower than ZIF-8/IL-CS MMMs and decreases at the highest loading under study. Membranes with 20 wt. % HKUST-1 were very fragile and full of defects, which made their characterisation more difficult than the others. The

16

glass transition temperature falls within the experimental error given the difficult observation of the midpoint in the second run curve of DSC analyses CS-based membrane samples [28], thus these values are not reported here.
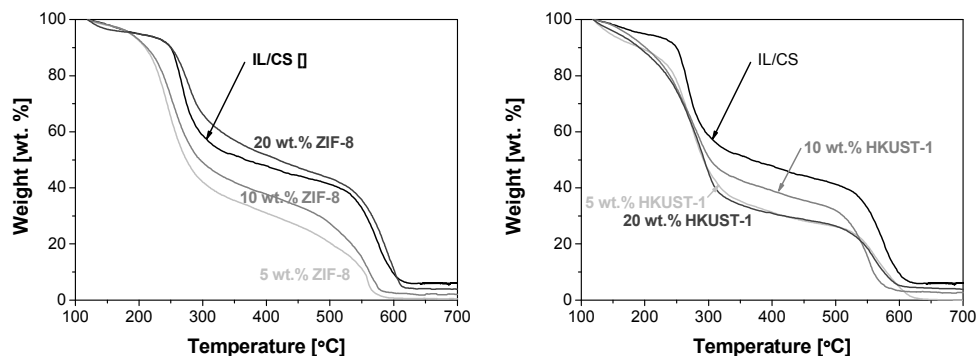

Figure 4. Thermogravimetric analyses of the IL-CS-based membranes using ZIF-8 and HKUST-1 fillers.

The dispersion and interaction between the components can also be observed after SEM in **Figure 5**. Even at the low loading of 5 wt. %, there is HKUST-1 particle sedimentation at the bottom during evaporation. However, the EDX mapping of 20 wt. % MOF and ZIF/IL-CS MMMs (because of the difficulty of observing lower loadings) in **Figure 6(a)** shows that the Cu presence is homogeneous all over the membrane matrix at a value of 19.63 ± 2.7 wt. %, although not so uniformly as in ZIF-8-based membranes in **Figure 6(b)**. In the case of ZIF-8, EDX reveal a homogeneous dispersion of Zn all over the membrane matrix area and thickness, with an average value of 17.7 ± 0.1 wt. % Zn. These values agree with the nominal loading of the MOF and ZIF in the MMMs. Since we cannot easily discern the nanometre size ZIF-8 particles by SEM, the image at 5 wt. % ZIF-8 is omitted from **Figure 5**.
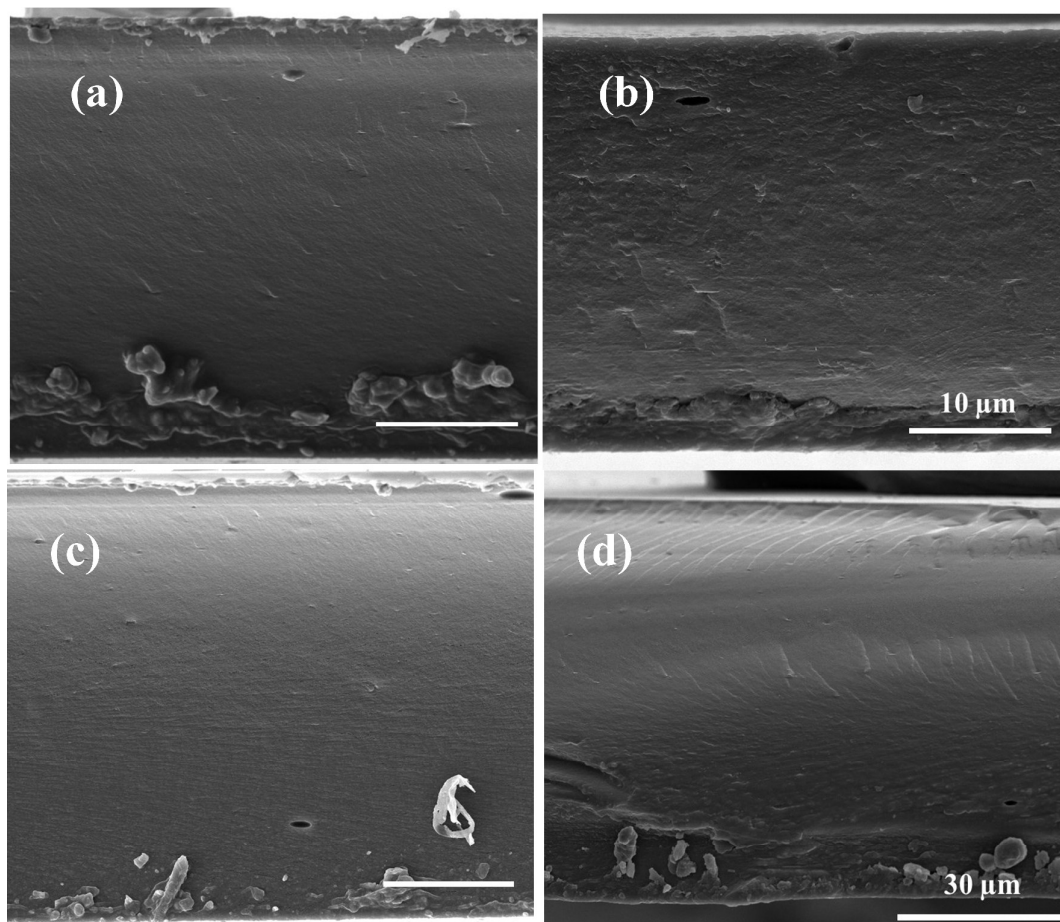
Figure 5. SEM images of the cross sectional area of IL-CS-based MMMs filled by (a) 5 wt. % HKUST-1 and (b) 20 wt. % HKUST-1, and (c) 10 wt. % ZIF-8 and 20 wt. % ZIF-8, respectively. Scale bar corresponds to 20 μm unless otherwise stated.

(a)   (b)
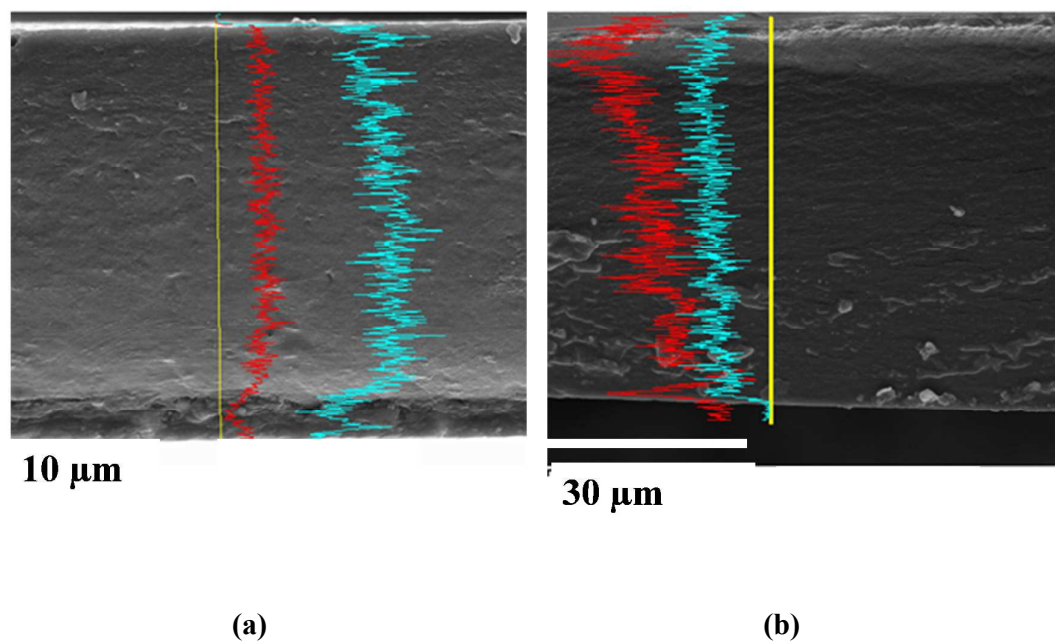
Figure 6. Electron images of HKUST-1 (a) and ZIF-8 (b) based IL-CS MMMs, at 20 wt. % particle loading.

Table 2. Morphological properties of ZIF-8/IL-CS membranes: Measured density (ρ_m), void volume fraction (ϕ_v), calculated as in eq. (2), as well as thermal decomposition measure by TGA (Fig. 4), and total water uptake (eq. 1).

Membrane materials	Thickness (μm)	ρ_m (g/cm^3)	ϕ_v (%)	T_d (^oC)	Water uptake (%)
CS [28]	122 ± 4	0.73 ± 0.26	23	188	111±29
IL/CS [28]	128 ± 4	1.11 ± 0.20	-	195	93±21
5 wt. % ZIF-8/IL-CS	90.4 ± 13	1.05 ± 0.08	37 ± 2.2	168 ± 32	58±5
10 wt. % ZIF-8/IL-CS	115 ± 5.2	1.09 ± 0.27	36 ± 10	185 ± 1.8	48±6

19

Membrane materials	Thickness (µm)	ρ_m (g/cm³)	ϕ_v (%)	T_d (ºC)	Water uptake (%)
20 wt. % ZIF-8/IL-CS	125 ± 12	0.96 ± 0.26	24 ± 13	186 ± 15	26±5
5 wt.% HKUST-1/IL-CS	91.8 ± 2.7	1.09 ± 0.19	49 ± 9	146 ± 1.8	79±29
10 wt. % HKUST-1/IL-CS	120 ± 5.2	1.21 ± 0.46	42 ± 8	169 ± 27	69±24
20 wt. % HKUST-1/IL-CS	146 ± 9.3	1.10 ± 0.26	33 ± 7	155 ± 6	57±35

The void volume fraction is a measure of the free volume that will be used to calculate the true volume fraction of the ZIF-8 or HKUST-1 filler particles dispersed in the MMM, to account for non-idealities in gas separation performance, as will be shown below. As observed in **Table 2**, the void volume fraction decreased with both ZIF-8 and HKUST-1 content. The water uptake, which is a measure of hydrophilicity and swelling of the membrane calculated by eq. (1), followed the same trend as the void volume fraction and thermal decomposition, in agreement with Bushell *et al.* for ZIF-8/PIM-1 MMMs [53].

The temperature does not affect the gas permeation through the IL-CS hybrid membranes used as base continuous membrane matrix in this work, in the range under study (25 – 50 ºC) [26]. In **Figure 7**, the permeability and selectivity of the membranes under study are plotted against the Robeson's upper bound and including values in the temperature range from 25 to 50 ºC.

The highest CO_2 permeability and CO_2/N_2 ideal selectivity were obtained for 10 wt. % ZIF-8 and 5 wt. % HKUST-1 /IL-CS membranes, as 5413 ± 191 Barrer and 11.5, and 4754 ± 1388 Barrer and 19.3, respectively, at 50 ºC and 2 bar. ZIF-8/PEBAX MMMs of similar morphology gave a maximum 1300 Barrer CO_2 and CO_2/N_2 selectivity of 32.3 at 25ºC and 2.6 bar, at the high ZIF-8 loading of 35% [40]. Hao *et al.* [29] reported, for the 3-phase ZIF-8/RTIL/PIL MMM, a CO_2 permeability of 902.4 Barrer and a CO_2/N_2 selectivity of 21, at 35ºC and 3.5 bar, for the high loading of 25.8 wt. %. The performance of HKUST-1 membranes is similar as expected given the fact that the small triangular windows connecting the main channels and the unsaturated Cu atom in tetrahedral pockets (0.35 nm) is very similar to the pore size of ZIF-8 (0.34 nm) [59]. The nominal loading at which defects appear differ for ZIF-8 or HKUST-1/IL-CS MMMs because of the poorer interfacial contact of HKUST-1 than ZIF-8. Although the CO_2/N_2 ideal selectivity obtained in this work is low, the separation performance of 10 wt.% ZIF-8 and 5 wt. %HKUST-1/IL-CS MMMs increases with filler and temperature, thus differing from the IL/CS membranes [26], where the CO_2/N_2 selectivity was 4.25 ± 0.5 and independent of temperature in the range under study.

The increase in permselectivity is attributed to the good adhesion and compatibility between the IL, the microporous particles and the polymer matrix [29], in agreement with the R_a interaction distances calculated from HSPs (see Table 1). The compatibility between MOF and polymer matrix is higher for the IL-CS hybrid matrix than the pristine CS polymer, and 2-component MOF/CS MMMs did not surpass an ideal CO_2/N_2 selectivity of around 2 (not shown). The best permselectivity is obtained at higher ZIF-8 loadings (10 – 20 wt.%) than HKUST-1 (5 wt. %), because the affinity of HKUST-1 with IL and CS is lower than that of ZIF-8, as discussed above.
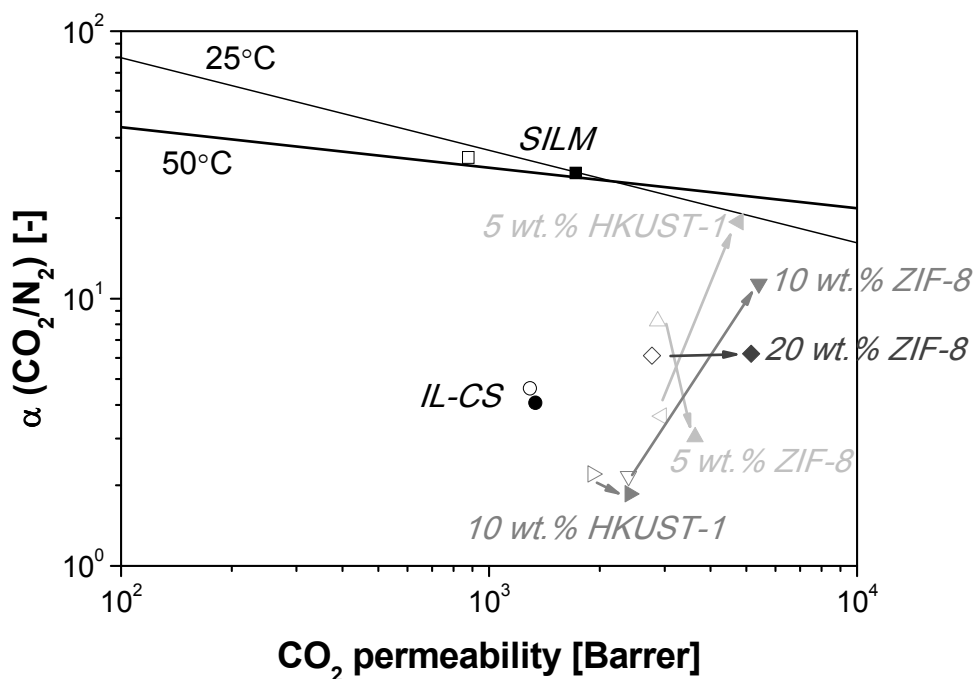
Figure 7. IL/CS-based membranes versus Robeson's upper bound for the CO_2/N_2 gas pair separation at 25ºC [7] and 50ºC with different loadings of HKUST-1 (5, 10 wt.%) and ZIF-8 (5, 10, 20 wt.%). Supported Ionic Liquid Membrane (SILM) data are collected from Santos *et al*. [25], and RTIL/CS hybrid membranes from Santos *et al*. [26] for comparison purposes. Temperature = 25ºC (void symbols) and 50 ºC (full symbols). Arrows show the evolution of each membrane material with increasing temperature.

The influence of temperature through novel MMMs at increasing filler loading is probably due to the creation of bypassing channels connecting the voids existing between the dispersed particles and the continuous matrix. The following study aims to observe how the temperature affects gas permeation from the point of view of the compatibility and adhesion of the components on membrane performance. In order to analyse the effect of temperature on membrane morphology and performance, several theoretical models are available to validate mathematically the gas transport properties of MMMs. Many researchers have tried to understand the influence of the morphology

22

of MMMs on their separation performance, based only on the interaction between the phases, and several reviews have been published recently to compare the different models [60-62], with their advantages and limitations, especially using glassy polymers and zeolite filler particles [63].

The most generalized models are those based on Maxwell equations, which have been recently extended to 3-phase MMM consisting of the dispersion of a small amount of solid dispersed fillers in a continuous polymer matrix and introducing an ionic liquid as liquid phase to improve the interaction among the other phases [15,29].

Maxwell model is the most commonly used to predict the permeability through a dilute suspension of spherical fillers in a continuous polymer matrix, by the following equation [64],

$$P_{eff} = P_c \left[\frac{nP_d + (1-n)P_c - (1-n)\phi_d(P_c - P_d)}{nP_d + (1-n)P_c + n\phi_d(P_c - P_d)} \right] \quad (10)$$

The general assumption when the fillers can be estimated as ideal spherical-like inserts, as is the case of IL, ZIF-8 and HKUST-1 in the present work, is $n = 1/3$, which converts eq. (10) to the most popular expression of Maxwell model,

$$P_{eff} = P_c \left[\frac{P_d + 2P_c - 2\phi_d(P_c - P_d)}{P_d + 2P_c + \phi_d(P_c - P_d)} \right] \quad (11)$$

where ϕ_d is the volume fraction of the filler in the MMM.

When $n = 1$, eq. (10) corresponds to the mass transport takes place by a series mechanism through the phases,

$$P_{eff} = \frac{P_c P_d}{\phi_c P_d + \phi_d P_c} \quad (12)$$

where P_c and P_d are the single component permeabilities of the polymer and filler phases.

When n = 0, eq. (10) describes the effective permeability through the MMM usually takes into account a two-layer transport mechanism, that is, both phases are supposed to work in parallel to the flow direction, as

$$P_{eff} = P_c \phi_c + P_d \phi_d \qquad (13)$$

The density values of the single components in the MMMs is 1.43 g/cm^3 for CS [6], 1.03 g/cm^3 [65] for the IL. The densities considered for the ZIF-8 and HKUST-1 dispersed particles are the calculated crystallographic values, 0.93 and 1.032 g/cm^3, respectively. For the 3-phase MMM reported in this work, P_c is the permeability measured through the IL-CS based membranes as reported in a previous work [26] and P_d is taken from the literature on pure ZIF-8 membrane layers, as 4390 and 180 Barrer for CO_2 and N_2, respectively [53]. For HKUST-1-IL/CS MMM, the P_d values are taken from Varela-Guerrero *et al.* [66], as 37313 and 2985 Barrer for CO_2 and N_2, respectively.

ϕ_d is the true filler volume fraction calculated from the void fraction in **Table 2** and the nominal filler volume fraction obtained from the densities of the components and the composition of the casting solution,

$$\phi_d = \phi_d^N \left(1 - \phi_v\right) \qquad (14)$$

The accuracy of these model equations to adjust the experimental data are evaluated by the minimized average absolute error, AARE, between the calculated and experimental permeability for CO_2 and N_2, respectively, as

$$\%AARE = \frac{100}{NDP} \sum_{i=1}^{NDP} \left| \frac{P_i^{calc} - P_i^{exp}}{P_i^{exp}} \right| \qquad (15)$$

where NDP is the number of data points, which in this work is taken as 2-3, to consider only the reproducible experimental runs.

We have observed that these simple Maxwell equations only provide an acceptable prediction in the case of N_2 permeability, which may be due to the sensitivity of the permeation measurement, *i.e.* N_2 permeability is much lower than CO_2 permeability. In general, the AARE is an average of 20% for IL/CS hybrid membranes and 40 % for ZIF-8 and HKUST-1-filled IL/CS MMMs, slightly reduced upon increasing temperature from 25 to 50 ºC.

Therefore, we have applied the extended modified Maxwell equation to grasp the influence of the interparticle distance and compatibility of the materials, as well as other non-idealities such as gas molecular size, polymer chain rigidification [67], pore-blockage [68] or the crystallinity [64] of the polymer matrix when introducing porous inorganic particles into a semi-crystalline polymer as continuous matrix. The modified model considers a three pseudo-phase system accounting for the inorganic dispersed filler, the polymer continuous matrix and the interface voids. The permeability P_{3MM} of this system is obtained by applying eq. (11) twice, first to predict the permeability through the "pseudo-insert" phase,

$$P_{eff} = P_I \left[\frac{P_d + 2P_I - 2\phi_s \left(P_I - P_d \right)}{P_d + 2P_I + \phi_s \left(P_I - P_d \right)} \right] \tag{16}$$

where P_I is the permeability of the interphase, and ϕ_s is the volume fraction of the insert phase within the "pseudo-insert" phase, given by

$$\phi_s = \frac{\phi_d}{\phi_d + \phi_I} = \frac{r_d^3}{\left(r_d + \ell_I \right)^3} \tag{17}$$

Here, ϕ_d and ϕ_I are the overall volume fraction in the membrane of the insert and the interphase, respectively; r_d is the insert radius and the interphase thickness is denoted ℓ_I. The value of the "pseudo-insert" permeability P_{eff} in eq. (16) is used again in

Maxwell's model, to predict permeability P_{3MM} for the three-phase mixed matrix materials,

$$P_{3MM} = P_M \left[\frac{P_{eff} + 2P_c - 2(\phi_d + \phi_I)(P_c - P_{eff})}{P_{eff} + 2P_c + (\phi_d + \phi_I)(P_c - P_{eff})} \right] \tag{18}$$

As $\phi_d + \phi_I$ approaches unity, the interphases of neighbouring insert particles overlap and the whole matrix is rigidified, leading to effective properties differing from the pure polymer. This chain rigidification is represented by the phenomenological parameter β, which in single gas permeation depends upon the nature of the gas molecule [68].

The semicrystalline nature of the base polymer is taken into account by a factor α, the volume fraction of the amorphous polymer responsible for gas transport,

$$\alpha = 1 - \chi \tag{19}$$

where χ is the crystallinity of the IL/CS hybrid membrane, measured as 0.18 from the FTIR spectrum [28].

$$P = S \times D = S^* \times D^* \times \alpha^2 = P^* \times \alpha^2 \tag{20}$$

The P_c in equation (21) is replaced by the P^* obtained in eq. (20). Likewise, the interphase permeability, P_I, in eq. (16), accounting for the immobilization factor to represent the degree of rigidification in the inter-crystalline amorphous segments is now defined as,

$$P_c = P_c^* \alpha^2 / \beta \tag{21}$$

in order to consider the amorphous region that is the permeable region of the MMM.

Figure 8 compares the calculated and experimental permeabilities as a function of temperature using this extended Maxwell model with the effect of the ZIF-8 particle size and loading as dispersed phase and the crystallinity of the hybrid IL/CS matrix as

26

continuous phase. In this case, the AARE is below 0.07% in all cases. The phenomenological parameters describing the interphase thickness, l_I (μm), and immobilisation or rigidification factor, β, estimated from the minimisation of these AARE values, are collected in **Table 3**.

(a)   (b)
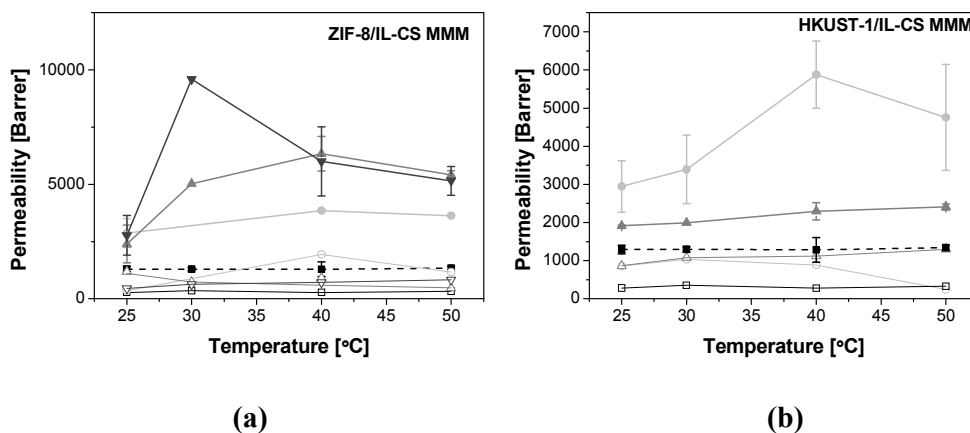
Figure 8. Experimental CO_2 (■) and N_2 (●) permeability through ZIF-8/IL-CS MMMs at different loadings: 0 (Black), 5 (Light grey), 10 (Grey), 20 (Dark grey) wt. %, respectively) (a) and HKUST-1/IL-CS MMMs: 5 (Black) and 10 (Grey) (b). Lines correspond to extended modified model predictions after equations (19-24): thick lines to CO_2 and thin lines to N_2 calculated permeabilities, respectively. Error bands are added to CO_2 permeability only for clarification purposes.

Table 3. Phenomenological parameters estimated by eqs. (12)-(21) as a function of ZIF-8 or HKUST-1 loading and working temperature.

T (ºC)	l_I (μm)	$\beta(CO_2)$ (-)	$\beta(N_2)$ (-)
5 wt.% ZIF-8/IL-CS MMMs			
25	0.20	1.095	0.77
40	0.20	0.80	0.06

50	0.20	0.88	0.27
10 wt.% ZIF-8/IL-CS MMMs			
25	0.15	0.46	0.23
30	0.15	0.25	0.46
40	0.15	0.19	0.44
50	0.15	0.24	0.66
20 wt.% ZIF-8/IL-CS MMMs			
25	0.10	0.51	0.58
30	0.10	0.16	0.52
40	0.10	0.24	0.37
50	0.10	0.28	0.38
5 wt.% HKUST-1/IL-CS MMMs			
25	0.46	0.37	0.34
30	0.46	0.40	0.36
40	0.46	0.23	0.32
50	0.46	0.30	1.40
10 wt.% HKUST-1/IL-CS MMMs			
25	0.46	0.72	0.34
30	0.46	0.69	0.35
40	0.46	0.59	0.26
50	0.46	0.59	0.27

The interphase distances are independent of temperature and have values much lower than reported in the literature for zeolite-PES MMMs [69], ITQ-29-polysulfone MMMs [70] or ZIF-20-polysulfone MMMs [71]. This correlates with the relatively good

28

compatibility of the chosen dispersed and continuous phases as hinted above by the Hansen' solubility theory. Although the R_a is somehow high compared to literature, the ZIF-8 is as soluble in IL as in CS, in a larger degree than HKUST-1, suggesting a better affinity between ZIF-8 than HKUST-1 and the IL-CS hybrid matrix contradicts the CO_2 permeation performance of a membrane based in a semi-crystalline polymer [26]. The interphase distance for HKUST-1/IL-CS MMM at only 5 wt. % particle loading is higher than the value obtained for the organic hybrid IL-CS matrix and this explains why no good membranes with this MOF could be processed at higher loadings. The chain immobilisation factors are very low for the IL-CS hybrid membranes, due to the good compatibility between IL and CS components, and they generally increase upon ZIF-8 loading, thus accounting for the rigidification that the ordered porous structure imparts to the continuous matrix. The interphase distance between the porous fillers and the continuous ionic polymer matrix predicted by this model agrees with other three-phase MMMs reported in the literature. Although in those cases where the continuous phase was composed of an ionic polymer and a room temperature IL, and SAPO-34 zeolite [15,16] or ZIF-8 [29] as dispersed phases, the l_l and $\beta(CO_2)$ and $\beta(N_2)$ are larger than in the present work. We have also considered the crystallinity of the continuous matrix [64], which decreases with the addition of even a small amount of IL [28].

As pointed out before, the IL may be acting as wetting medium between the ZIF-8 or HKUST-1 particles and the IL-CS hybrid matrix, since the R_a distance between ZIF-8 or HKUST-1 with IL-CS material diminishes from the Ra distance with the pristine CS polymer, as calculated in **Table 1**. The good adhesion between the IL-CS continuous matrix and the ZIF-8 nanoparticles is slightly better than for the HKUST-1 nanoparticles, because of the similarity between ZIF-8 and the IL. This reason, together with the higher particle size of HKUST-1 causes that the best permselectivity of

HKUST-1-based IL-CS MMMs is achieved at lower (5 wt. %) loading than ZIF-8-based MMMs.

Conclusions

Three-component MMMs were prepared by adding a highly CO_2 absorbing non-toxic ionic liquid, [emim][Ac] (IL), a biopolymer from abundant natural resources, chitosan (CS), and MOF ZIF-8 or HKUST-1 nanoparticles to improve the selectivity of the IL-CS hybrid continuous polymer matrix. The increasing amount of ZIF-8 and HKUST-1 does not deteriorate the thermal stability of the hybrid IL-CS membranes. which allows expecting the potential of such materials for developing high temperature resistant membrane materials for CO_2 separation. This, together with the fact that the water content in the membrane is constant before and after the whole set of permeation runs allows expecting the potential of such materials for developing high temperature resistant membrane materials for CO_2 separation The influence of the temperature and MMMs morphology on CO_2/N_2 separation performance was analysed. The adhesion between the phases in terms of the gas transport properties was interpreted by Hansen solubility parameters (HSP) and Maxwell-based models, modified to account for chain rigidification, pore blockage and crystallinity of the IL-CS matrix, with very accurate predictions. In particular, HSP approach reveals better ZIF-8 compatibility with CS and IL than HKUST-1, and the preferential affinity of the chosen components towards CO_2 vs. N_2 is confirmed. The best permselectivity membranes are the 10 wt. % ZIF-8/IL-CS and the 5 wt.% HKUST-1/IL-CS MMMs, where the separation efficiency increases in the temperature range under study. This is due to the better affinity of ZIF-8, as predicted by HSP and confirmed by the extended modified Maxwell model with lower

interphase thicknesses and chain rigidification factor for ZIF-8 than HKUST-1. To obtain performance enhancement and enable scale up of the separation process, scale down of the selective layer thickness is necessary and thus composite membranes composed of a thin hybrid selective layer coated on a robust porous supports are being studied in the laboratory and their performance will be reported in a future work.

References

(1)   K. Ramasubramanian, Y. Zhao and W. S. W. Ho, *AIChE J.*, **2013**, *59*, 1033-1045.

(2)   C. Casado-Coterillo, T. Yokoo, T. Yoshioka, T. Tsuru and M. Asaeda, *Sep. Sci. Technol.*, **2011**, *46*, 1224-1230.

(3)   J. Gascón, F. Kapteijn, B. Zornoza, V. Sebastián, C. Casado and J. Coronas, *Chem. Mater.*, **2012**, *24*, 2829-2844.

(4)   L. Robeson, L. M. *J. Membr. Sci.* **2008**, *320*, 390-400.

(5)   Y. Huang, T. C. Merkel and R. W. Baker, *J. Membr. Sci.,* **2014**, *463*, 33.

(6)   J. K. Adewole, A. L. Ahmad, S. Ismail and C. P. Leo, *Int. J. Greenh. Gas Control*, **2013**, *17*, 46-65.

(7)   Z. Dai, R. Noble, D. L. Gin, X. Zhang and L. Deng, *J. Membr. Sci.*, **2016**, *497*, 1-20.

(8)   C. E. Powell and G. G. Qiao, *J. Membr. Sci.*, **2006**, *279*, 1-49..

(9)   H. Mushardt, V. Kramer, D. Hülagü, T. Brinkmann and M. Kraume, *Chem. Ing. Tech.*, **2013**, *86*, 83-91.

(10)   J. Caro and M. Noack, *Micropor. Mesopor. Mat.*, **2008**, *115*, 215-233..

(11)   M. Rezakazemi, A. E. Amooghin, M. M. Montazer-Rahmati, A. F. Ismail and T. Matsuura, *Prog. Pol. Sci.*, **2014**, *39*, 817-861.

(12)   L. C. Tomé, D. J. S. Patinha, R. Ferreira, H. García, C. S. Pereira, C. S. R. Freire, L. P. N. Rebelo and I. M. Marrucho, *ChemSusChem*, **2014**, *7*, 110-113..

(13)   L. Gómez-Coma, A. Garea and A. Irabien, *Sep. Purif. Technol.*, **2014**, *132*, 120-125.

(14)   M. Alvarez-Guerra and A. Irabien, *Green Chem.*, **2011**, *13*, 1507-1516.

(15)   Y. C. Hudiono, T. K. Carlisle, A. L. LaFrate, D. L. Gin and R. D. Noble, *J. Membr. Sci.*, **2011**, *370*, 141-148.

(16)   D. F. Mohshim, H. Mukhtar and Z. Man, *Sep. Purif. Technol.*, **2014**, *135*, 252-258.

(17)   Kumbharkar, S. C.; Bhavsar, R. S.; Kharul, U. K. *RSC Adv*. **2014**, *4*, 4500.

(18)   Adzima, B. J.; Venna, S. R.; Klara, S. S.; He, H.; Zhong, M.; Luebke, D. R.; Mauter, M. S.; Matyjaszewski, K.; Nulwala, H. B. *J. Mater. Chem. A* **2014**, *2*, 7967.

(19)   L. Liu, A. Chakma and X. Feng, *J. Membr. Sci.*, **2008**, *310*, 66-75.

(20)   L. A. El-Azzami and E. A. Grulke, *Ind. Eng. Chem. Res.*, **2009**, *48*, 894-902.

(21)   T. Kai, T. Kouketsu, S. Duan, S. Kazama and K. Yamada, *Sep. Purif. Technol.*, **2008**, *63*, 524-530.

(22)   S. Xiao, X. Feng and R. Y. M. Huang, *J. Membr. Sci.*, **2007**, *306*, 36-46.

(23)   M. B. Patil and T. M. Aminabhavi, *Sep. Purif. Technol.*, **2008**, *62*, 128-136.

(24)   Ding, Z.-D.; Chi, Z.; Gu, W.-X.; Gu, S.-M.; Liu, J.-H.; Wang, H.-J. *Carbohydr. Polym.* **2012**, *89*, 7.

(25)   E. Santos, J. Albo and A. Irabien, *J. Membr. Sci.* **2014**, *452*, 277-283.

(26)   Santos, E.; Rodríguez-Fernández, E.; Casado-Coterillo, C.; Irabien, A. *Int. J. Chem. React. Eng.* **2015**, *13*.

(27)   S.-C. Lu and I. F. J. Vankelecom, *React. Funct. Polym.*, **2015**, *86*, 117-124.

(28)   C. Casado-Coterillo, M. d. M. López-Guerrero and A. Irabien, *Membranes*, **2014**, *4*, 287-301.

(29)   L. Hao, P. Li, T. Yang and T.-S. Chung, *J. Membr. Sci.*, **2013**, *436*, 221-231.

(30)   B. Zornoza, C. Tellez, J. Coronas, J. Gascon and F. Kapteijn, *Micropor. Mesopor. Mat.*, **2013**, *166*, 67-78.

(31)   R. Adams, C. Carson, J. Ward, R. Tannenbaum and W. Koros, *Micropor. Mesopor. Mat.*, **2010**, *131*, 13-20.

(32)   S. S.-Y. Chui, S. M.-F. Lo, J. P. H. Charmant, A. G. Orpen and I. D. Williams, *Science*, **1999**, *283*, 1148-1150.

(33)   A. Car, C. Stropnik and K.-V. Peinemann, *Desal.*, **2006**, *200*, 424-426.

(34)   G. Yilmaz and S. Keskin, *J. Membr. Sci.*, **2014**, *454*, 407-417.

(35)   Q. Song, S. K. Nataraj, M. V. Roussenova, J. C. Tan, D. J. Hughes, W. Li, P. Bourgoin, M. A. Alam, A. K. Cheetham, S. A. Al-Muhtaseb and E. Sivaniah, *Energy Environ. Sci.,* **2012**, 5, 8359-8369.

(36)   S. Shahid and K. Nijmeijer*, J. Membr. Sci.*, **2014**, *470*, 166-177.

(37)   Y. Dai, J. R. Johnson, O. Karvan, D. S. Sholl and W. J. Koros, *J. Membr. Sci.*, **2012**, *401-402*, 76-82.

(38)   Z. Zhang, S. Xian, Q. Xia, H. Wang, Z. Li and J. Li, *AIChE J.*, **2013**, *59*, 2195-2206.

(39)   T. Li, Y. Pan, K.-V. Peinemann and Z. Lai, *J. Membr. Sci.*, **2013**, *425-426*, 235-242.

(40)   V. Nafisi and M.-B. Hägg, *J. Membr. Sci.*, **2014**, *459*, 244-255.

(41)   F. D. Silva, G. Magalhaes, E. Jardim, J. Silvestsre-Albero, A. Sepúlveda-Escribano, D. D. Azevedo and S. D. Lucena, *Ads. Sci. Technol.*, **2015**, *33*, 223-242.

(42)   Vicent-Luna, J. M.; Gutiérrez-Sevillano, J. J.; Anta, J. A.; Calero, S. *The Journal of Physical Chemistry C* **2013**, *117*, 20762.

(43)   N. A. H. M. Nordin, A. F. Ismail, A. Mustafa, R. S. Murali and T. Matsuura, *RSC Adv.*, **2014**, *4*, 52530-52541..

(44)   Y. Pan, Y. Liu, G. Zeng, L. Z. hao and Z. Lai, *Chem. Comm.*, **2011**, *47*, 2071-2073.

(45)   P. Burmann, B. Zornoza, C. Téllez and J. Coronas, *Chem. Eng. Sci.*, **2014**, *107*, 66-75.

(46)   L. H. Wee, M. R. Lohe, N. Janssens, S. Kaskel and J. A. Martens, *J. Mater. Chem.*, **2012**, 22, 13742-13746.

(47)   S. Sorribas, A. Kudasheva, E. Almendro, B. Zornoza, O. Iglesia, C. Téllez and J. Coronas, *Chem. Eng. Sci.*, **2015**, *124*, 37-44.

(48)   Cussler, E. L. *Diffusion. Mass transfer in fluid systems*; 3rd ed.; Cambridge University Press: Cambridge, 2007.

(49)   Zhu-Ryberg, Y. Z.; Edlund, U.; Albertsson, A.-C. *Biomacromol.* **2011**, *12*, 1355.

(50)   Hansen, C. M.; CRC Pres: Boca Raton, 2007, p 546pp.

(51)   Xie, H.; Zhang, S.; Li, S. *Green Chem.* **2006**, *8*, 630.

(52)   Casettari, L.; Vllasaliu, D.; Castagnino, E.; Stolnik, S.; Howdle, S.; Illum, L. *Prog. Pol. Sci.* **2012**, *37*, 659.

(53)   A. F. Bushell, M. P. Attfield, C. R. Mason, P. M. Budd, Y. Yampolskii, L. Starannikova, A. Rebrov, F. Bazzarelli, P. Bernardo, J. C. Jansen, M. Lanc, K. Friess, V. Shantarovich, V. Gustov and V. Isaeva, *J. Membr. Sci.*, **2013**, *427*, 48-62.

(54)   M. J. C. Ordoñez, K. J. B. Jr., J. P. Ferraris and I. H. Musselman, *J. Membr. Sci.*, **2010**, *361*, 28-37.

(55)   Weerachanchai, P.; Wong, Y.; Lim, K. H.; Tan, T. T. Y.; Lee, J.-M. *ChemPhysChem* **2014**, *15*, 3580.

(56)   Elangovan, D.; Nidoni, U.; Yuzay, I. E.; Selke, S. E. M.; Auras, R. *Ind. Eng. Chem. Res.* **2011**, *50*, 11136.

(57)   Paseta, L.; Potier, G.; Abbott, S.; Coronas, J. *Org. Biomol. Chem.* **2015**, *13*, 1724.

(58)   Wang, J.; Zheng, X.; Wu, H.; Zheng, B.; Jiang, Z.; Hao, X.; Wang, B. *J. Power Sources* **2008**, *178*, 9.

(59)   S. Basu, A. Cano-Odena and I. F. J. Vankelecom, *Sep. Purif. Technol.*, **2011**, *81*, 31-40.

(60)   Vinh-Thang, H.; Kaliaguine, S. *Chem. Rev.* **2013**, *113*, 4980.

(61)   Shen, Y.; Lua, A. C. *AIChE J.* **2013**, *59*, 4715.

(62)   Shimekit, B.; Mukhtar, H.; Murugesan, T. *J. Membr. Sci.* **2011**, *373*, 152.

(63)   Hashemifard, S. A.; Ismail, A. F.; Matsuura, T. *J. Membr. Sci.* **2010**, *347*, 53.

(64)   Shen, M.; Lin, Y. H. X.; Ding, B.; Zhang, L.; Zhang, X. *J. Appl. Pol. Sci.* **2013**, *127*, 2938.

(65)   Blath, J.; Deubler, N.; Hirth, T.; Schiestel, T. *Chem. Eng. J.* **2012**, *181-182*, 152.

(66)   Varela-Guerrero, V.; Yoo, Y.; McCarthy, M. C.; Jeong, H.-K. *J. Mater. Chem.* **2010**, *20*, 3938.

(67)   Moore, T. T.; Mahajan, R.; Vu, D. Q.; Koros, W. J. *AIChE J.* **2004**, *50*, 311.

(68)   Li, Y.; Guan, H.-M.; Chung, T.-S.; Kulprathipanja, S. *J. Membr. Sci.* **2006**, *275*, 17.

(69)   Casado-Coterillo, C.; Soto, J.; Jimaré, M. T.; Valencia, S.; Corma, A.; Téllez, C.; Coronas, J. *Chem. Eng. Sci.* **2012**, *73*, 116.

(70)   Seoane, B.; Zamaro, J. M.; Téllez, C.; Coronas, J. *RSC Adv.* **2011**, *1*, 917.
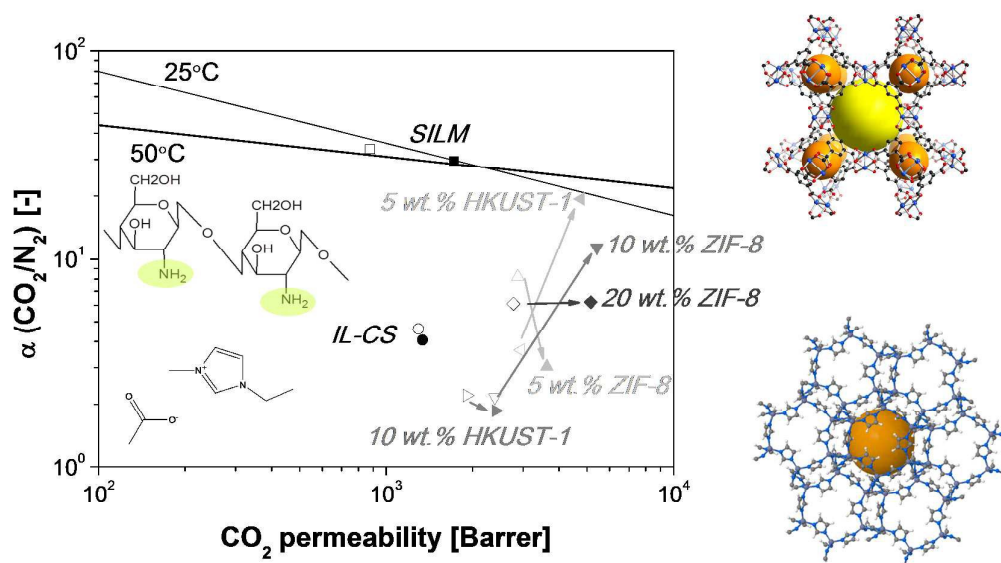
The CO_2 permeability and CO_2/N_2 selectivity of IL-CS hybrid membranes is improved by the addition of small quantities of HKUST-1 or ZIF-8 nanoparticles, in the range 25 – 50 ºC and the permselectivity is predicted accurately by Maxwell-derived models as a function of the good interfacial contact, crystallinity and pore blockage with temperature.